J. Synchrotron Rad. (1996). **3**, 75–83

A New Powder Diffractometer for Synchrotron Radiation with a Multiple-Detector System

H. Toraya,[a] H. Hibino[a] and K. Ohsumi[b]

[a]Ceramics Research Laboratory, Nagoya Institute of Technology, Asahigaoka, Tajimi 507, Japan, and [b]Photon Factory, National Laboratory for High-Energy Physics, Ohho, Tsukuba 305, Japan

(Received 10 October 1995; accepted 14 November 1995)

A new powder diffractometer for synchrotron radiation with six detector arms has been constructed. Five detector arms are attached radially at intervals of 25° to the 2θ axis and form a multiple-detector system. Five scintillation counters coupled with flat Ge(111) crystal analyzers on the respective arms can simultaneously record the whole powder pattern divided into five segments, each with an equal 2θ span. The optics design is based on flat-specimen reflection geometry using a parallel beam. The intensity data are collected using a 2θ step-scan technique in asymmetric diffraction at a fixed incident angle. A sixth multi-purpose detector arm can be used in the conventional single-arm scan mode. It can be equipped with various kinds of analyzers such as long horizontal parallel slits, a flat or channel-cut crystal analyzer, a receiving slit and a solid-state detector. Test operations of the multiple-detector system, conducted at the Photon Factory in Tsukuba, recorded a full width at half maximum of 0.022° and a peak maximum intensity of more than 40 000 counts s^{-1} for the (111) reflection from Si powder. The whole powder pattern of Mg_2SiO_4 over a 2θ range of 130° could be step-scanned at a step interval of 0.004° (2θ) in just 4 h. Results of whole-powder-pattern decomposition and Rietveld refinement of the Mg_2SiO_4 pattern are given.

Keywords: powder diffraction; detectors; magnesium silicate.

1. Introduction

Synchrotron radiation light sources have become indispensable for high-resolution powder diffraction experiments. A high-angular resolution of diffraction data is an essential factor for success in *ab initio* structure determination (Estermann & Gramlich, 1993). The sharp instrumental function makes the line-broadening effects arising from crystallite size and strain conspicuous (Cox, 1992). A symmetric and simple profile shape in powder diffraction using synchrotron radiation is very important in the accurate determination of peak positions and thus of unit-cell parameters (Hart, Cernik, Parrish & Toraya, 1990).

An angular resolution of 0.01–0.05° in full width at half maximum (FWHM) of the instrumental function can be easily obtained by parallel-beam optics using synchrotron radiation (Cox, 1992; Hart, 1992). It is higher by almost one order of magnitude compared with the angular resolution of an ordinary-type powder diffractometer using a laboratory X-ray source. Such high-resolution diffraction experiments, however, require much smaller step sizes, *e.g.* 0.002° in 2θ, to record a powder pattern (Finger, Cox & Jephcoat, 1994), and the scan time required for data collection becomes unduly long. For example, it would take 39 h for scanning the whole 2θ range of 140° even if we spent just 1 s counting at each step and another 1 s moving to the next step. The number of researchers who want to use synchrotron radiation facilities, and materials to be analyzed using synchrotron radiation are increasing in volume. The number of powder diffraction stations for synchrotron radiation is limited, however.

Imaging plates and position-sensitive detectors are suitable for integrated and fast data collection in the angle-dispersive mode (Barnea *et al.*, 1992). In these instruments, a capillary specimen is generally used in the Debye–Scherrer geometry. It is advantageous to use air-sensitive and small-volume samples (Evain, Deniard, Jouanneaux & Brec, 1993) and to reduce the preferred orientation, whereas the diffraction geometry cannot avoid the problems of X-ray absorption by sample materials containing heavy elements and the relatively high background scattering. On the other hand, advantages of diffractometer scans in the flat-specimen reflection geometry are (i) a wide range of angular resolution using different analyzers, (ii) accurate measurements of angular positions and intensities, and (iii) high counting rates and good particle statistics. Application to thin-film diffraction measurements is another aspect of our proposed research.

For solving the problem of prolonged experimental time in the diffractometer scan, a multiple-detector system has been devised. This new type of detector system can be realized by adopting an asymmetric 2θ-scan technique at a fixed incident angle in parallel-beam optics. Instrumental design and results of a test operation conducted at the Photon Factory in Tsukuba are described in the present paper.

2. Instrumentation

2.1. *Design concept*

Symmetric θ–2θ scan techniques are widely used for data collection with powder diffractometers. This seems to be due to the traditional reason that most powder diffractometers have adopted focusing geometry. For divergent beams, focusing geometry is a superior technique for obtaining intensity and resolution (Parrish, 1992). A symmetric arrangement of incident and diffracted beams against a flat specimen surface is required to satisfy focusing conditions on a constant goniometer radius.* Out of focus, the diffraction profile is broadened and degraded. In parallel-beam optics, however, specimen-displacement-type aberrations are eliminated (Hastings, Thomlinson & Cox, 1984) and the asymmetric 2θ scan at a fixed incident angle by decoupling θ and 2θ axes does not degrade the diffraction profile (Hart, Parrish, Bellotto & Lim, 1988; Hart, 1992; Toraya, Huang & Wu, 1993*a*). Thus, a number of detectors can be set at any 2θ angle on a goniometer circle, and can be operated simultaneously.

Two possible choices for the analyzer are to use a crystal analyzer or long horizontal parallel slits. The former is generally considered to give higher angular resolution and a good signal-to-noise ratio (Cox, Hastings, Cardoso & Finger, 1986), whilst the latter is advantageous in obtaining a higher diffracted intensity (Parrish & Hart, 1987). Moreover, it is not necessary to realign the optical axis for parallel slits each time when there is a change of wavelength, while the Bragg reflection angle of the analyzer crystal must be tuned with wavelength. Although this achromatic nature of parallel slits in instrumental alignment (Hart, 1991) is a great advantage for the multiple-detector system, the crystal analyzer has been adopted in the present system. One reason is that high angular resolution was considered to be important. Another is that the construction of several sets of long horizontal parallel slits with uniform efficiency was considered to be technically difficult at present.

Since the instrument is installed at a general user beamline, the diffractometer was designed to have two kinds of detector system on a goniometer. One is a multiple-detector system (hereafter called MDS) for scanning a whole powder pattern, and the other is a conventional-type single-detector system for multi-purpose use (MPA).

2.2. *Multiple-detector system*

A schematic diagram of the system is shown in Fig. 1 and a photograph of the diffractometer is shown in Fig. 2. Five detector arms for the MDS are attached radially to the 2θ axis of the rotary table (Franke PMD 400 for 2θ and PMD 265 for θ) at intervals of 25°, and are numbered 1–5 from the low-angle side. Each arm has Soller slits with an angular aperture of 2°, a flat Ge(111) crystal analyzer, adjustable anti-scatter baffle and a scintillation counter. The window of the scintillation counter, with an aperture of diameter 20 mm, is located 340 mm from the sample position. The Bragg angle of the analyzer crystal can be adjusted using a stepping motor. The crystal analyzers are covered with steel boxes in order to avoid interference with neighbouring analyzers. Rotation of the MDS by 25° in 2θ can measure the pattern over a 2θ range of 125°.

The MDS is normally used in the 2θ scan mode. Arm 5 of the MDS (Fig. 1) can be used alone, and operated in both 2θ and θ–2θ scan modes.

2.3. *Multi-purpose detector arm*

A sixth arm (MPA) is the multi-purpose detector arm (Fig. 1), which can be equipped with various types of analyzer. At present, two long horizontal parallel slits with angular apertures of 0.032 and 0.065°, which were

* The asymmetric arrangement of incident and diffracted beams for the goniometer with a constant goniometer radius is described by Kobayashi (1992).

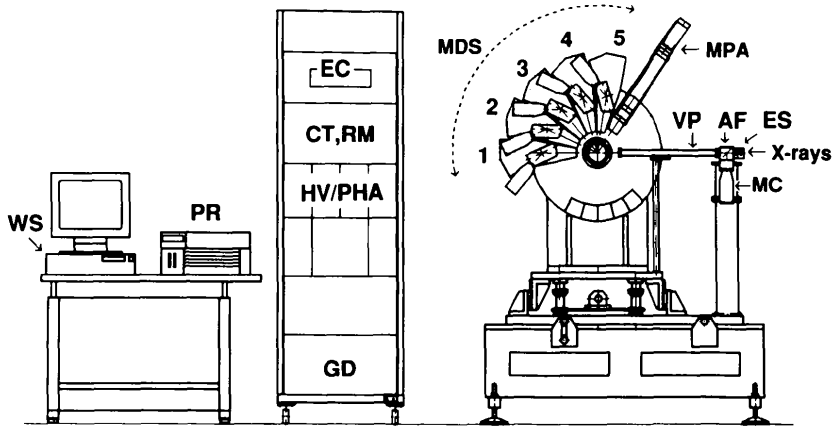

Figure 1
A schematic diagram of the system. MDS = multiple-detector system, MPA = multi-purpose detector arm, ES = entrance slits, AF = aluminium foil, MC = monitor scintillation counter, VP = vacuum path, EC = encoder counter, CT = counter timer, RM = rate meter, HV = high voltage, PHA = pulse-height analyzer, GD = goniometer driver, WS = workstation and PR = printer.

developed in a previous study (Toraya, Takata, Hibino, Yoshino & Ohsumi, 1995), and a set of receiving slits are available for use together with the Soller slits (angular aperture of 2°). Different types of flat and channel-cut crystals and a clasp for attaching a Peltier-type solid-state detector will be available for use by the end of 1995. This detector system can be operated in the conventional single-arm scan mode.

2.4. *Goniometer and entrance slits*

A minimal value for the reading of the Hedienhain encoder (RON-806) for the 2θ axis is 0.0001°, and the goniometer can be rotated by the same increment per pulse by a stepping motor.

The sizes of the incident beam in the vertical and horizontal directions are defined by two entrance slits (ES). Part of the incident beam is scattered downward by aluminium foil (AF) and its decay is monitored by a scintillation counter (MC). A vacuum path (VP) of length 457 mm helps to decrease the air scattering and to increase the intensity of the incident beam by more than 60% (for $\lambda = 1.54$ Å) with respect to the absorption of X-rays through air.

The bases for the goniometer and the entrance slit can be moved in the vertical direction with stepping motors (0.001 mm pulse^{-1}) separately or simultaneously in a synchronized motion.

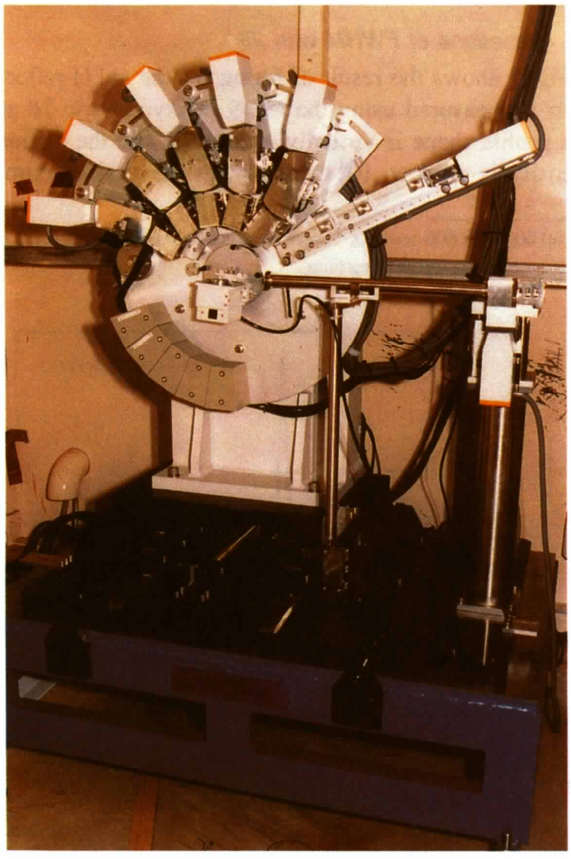

Figure 2
The diffractometer inside the hutch of the BL-4B experimental station at the Photon Factory.

2.5. *Electronic circuit and controller*

A standard-type high-voltage/pulse-height analyzer (Rigaku 5320C1) and scaler-timer units (Canberra 2071A-2072A) were installed in a console, as shown in Fig. 1.

All commands for system control can be selected from icons and menus in windows displayed on the CRT of the work station (Hewlett Packard 712/60). The whole system was constructed by the Rigaku Corporation.

3. Experimental

Diffractometer tests were conducted at the BL-4B experimental station at the Photon Factory. The diffractometer was installed at a distance of *ca* 20 m from a bending-magnet light source (positron energy of 2.5 GeV and beam current of 360–260 mA). A monochromatic non-focusing beam with a wavelength of 1.5416 Å was obtained using a water-cooled double-crystal Si(111) monochromator at a distance of 17.3 m from the light source. The optical axes of the entrance slits, goniometer, and the 2θ-zero of the MPA were first aligned using an attenuated direct beam. Each arm of the MDS was then aligned. It took just 20–30 min to align one MDS arm, which includes the tuning of the Bragg angle of the analyzer crystal, the 2θ-zero position, and the high-voltage/pulse-height analyzer.

National Institute of Standards and Technology (NIST) Standard Reference Material (SRM) 640b Si, SRM 674 CeO_2 and synthesized Mg_2SiO_4 powders were used as samples. They were packed into the hollow of the specimen holder of diameter 30 mm. For data collection, the beam sizes were enlarged to 1.5 mm in height and 15 mm in width. The profile intensity was step-scanned at a step interval of 0.002 or 0.004° and a counting time of 1 s at each step. The asymmetric 2θ scan mode was used for the MDS at a fixed incident angle of 5° for all specimens. The symmetric θ–2θ scan mode using arm 5 of the MDS was also employed for Si. The flat specimen was rotated in the plane of the specimen surface at 60 rotations min^{-1} during the scan.

4. Data analysis

Profile intensity data were first analyzed using the computer program *PRO-FIT* for individual profile fitting (Toraya, 1986). A split-type pseudo-Voigt function (Toraya, 1990) was used as the profile function, and a description of the fitting procedure can be found elsewhere (Toraya, 1986).

The whole powder pattern of Mg_2SiO_4 recorded with the MDS at a step interval of 0.004° in 2θ was also analyzed using the computer program *WPPF* for whole-powder-pattern decomposition (Toraya, 1986) and *PFLS* for Rietveld refinement (Toraya & Marumo, 1980). Five segments of a whole pattern, recorded with respective detector

Table 1
Results of testing the multiple-detector system using the (111) reflection from CeO_2.

Arm number	I_j	H_j	η_j
1	673 (2)	0.0254 (2)	0.71 (1)
	665 (3)	0.0255 (2)	0.70 (1)
2	646 (3)	0.0251 (2)	0.69 (1)
	637 (3)	0.0248 (2)	0.71 (1)
3	599 (3)	0.0249 (2)	0.64 (1)
	599 (3)	0.0246 (2)	0.65 (1)
4	637 (2)	0.0256 (2)	0.68 (1)
	639 (2)	0.0258 (2)	0.67 (1)
5	597 (3)	0.0248 (2)	0.65 (1)
	598 (3)	0.0247 (2)	0.65 (1)
Average	629 (29)	0.0251 (4)	0.67 (3)

arms of the MDS, were connected with the specially written computer program *PROCESS*. Small disagreements in peak position and intensity for the same reflections observed with the two adjacent detectors were adjusted by least squares using the data in the overlapping regions.

In the refinement with *WPPF*, the integrated intensity parameters for 265 independent reflections in the 2θ range 15–128° (28251 data points) were varied together with six background parameters in the fifth-order polynomial function, unit-cell parameters, the 2θ-zero point, the U, V and W parameters in the Caglioti, Paoletti & Ricci (1958) formula for the FWHM, asymmetry parameters (Toraya, 1986), and the linearly 2θ-varying η parameters in the pseudo-Voigt function.

In the Rietveld refinement, the same profile model as that used in the *WPPF* refinement was chosen, while the structural parameters of Mg_2SiO_4 were refined instead of adjusting the integrated intensity parameters. Initial atomic parameters for Mg_2SiO_4 were those given by Lager, Ross, Rotella & Jorgensen (1981). The f, f' and f'' tables for Mg^{2+} and Si^{4+} were taken from *International Tables for X-ray Crystallography* (1974) and an f table for O^{2-} given by Tokonami (1965). The integrated intensity was corrected for Lorentz and polarization effects (Cox, 1992), the intensity enhancement in asymmetric diffraction (Toraya, Huang & Wu, 1993*b*), the intensity reduction arising from the limited dimensions of the detector system, and the preferred orientation. The preferred orientation was corrected by the function of symmetrized harmonics expansion (Järvinen, 1993).

5. Results

5.1. *Uniformity and reproducibility tests of the MDS*

Table 1 gives some profile parameters for the (111) reflection from CeO_2, intensity data of which were measured successively using each of the respective arms of the MDS. Two sets of intensity data were obtained on two different days, and results for the later scan are given on the second lines in Table 1. An average value for the integrated intensity (I_j) was obtained after correcting for the decay of the incident beam using monitor counts. Numbers in parentheses for each parameter are the estimated standard deviations (e.s.d.'s) as an output from the least-squares fitting, and those for averages were mean deviations (m.d.'s) given by $[\sum(x_j - x_{mean})^2/(n-1)]^{1/2}$. The m.d. for I_j is 4.6% while those for the profile width (H_j) and shape (η_j) are 1.7 and 3.8%, respectively. These m.d. values can be further reduced by carefully aligning the tilt of the analyzer crystal. The difference between the two I_j values for the same arm is, however, much smaller, being within the e.s.d. for arms 3–5 and less than three times the e.s.d. for arms 1 and 2. These differences are 1.4% at maximum and 0.6% on average. Good reproducible integrated intensities were obtained, and the difference in the efficiency of analyzer–counter systems among the five detectors could be reliably corrected.

5.2. *Intensity enhancement in asymmetric diffraction*

The diffracted intensity in asymmetric diffraction is enhanced compared with that in symmetric diffraction, and its intensity ratio is given by $2/(1 + \sin\alpha/\sin\beta)$ (Toraya *et al.*, 1993*b*). The observed intensity ratio for the (111) reflection from Si was 1.61, and agrees well with the calculated value of 1.64. An intensity of 41 177 counts s^{-1}* was recorded for the (111) reflection from Si in the asymmetric scan.

5.3. *Variations of FWHM with 2θ*

Fig. 3 shows the result of fitting for the (111) reflection from Si measured using the MDS in asymmetric 2θ scan. The profile shape is virtually symmetric and the diffracted intensity is *ca* 3×10^4 counts s^{-1} at the peak maximum.

* 100 000–120 000 counts s^{-1} were recorded in recent experiments using a focusing mirror on the beamline.

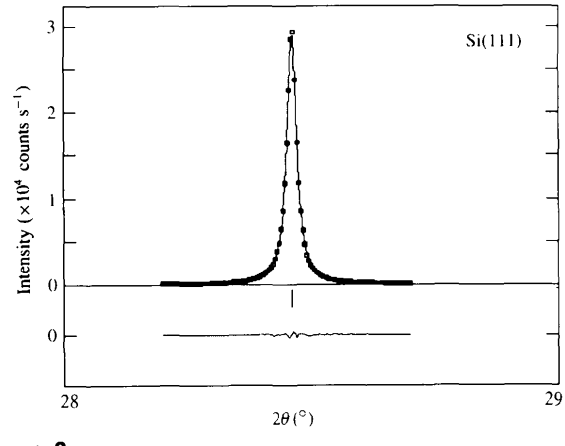

Figure 3
Fit for the (111) reflection from Si measured using the multiple-detector system in asymmetric 2θ scan mode. Open squares represent the observed intensity, the solid line the calculated intensity, and the difference plot is given at the bottom of the diagram. A short vertical bar represents a Bragg reflection position.

Fig. 4 shows a variation of the FWHM of the reflections from Si with 2θ, measured using asymmetric (solid squares) and symmetric (open squares) scans. The minimum FWHM values are 0.0221 (2) and 0.0216 (2)° for asymmetric and symmetric scans, respectively. Numbers (1 to 5) shown along the plots in Fig. 4 correspond to those of the MDS arms in Fig. 1. The plots of FWHM observed by asymmetric scan using five different detectors lie on a smooth curve. The formulae for FWHM, which were least-squares fitted to the observed data, were $H(2\theta) = (0.00142\tan^2\theta - 0.00042\tan\theta + 0.00056)^{1/2}$ and $H(2\theta) = (0.00187\tan^2\theta - 0.00059\tan\theta + 0.00054)^{1/2}$ for asymmetric and symmetric scans, respectively. The FWHM were almost the same, as expected, for both data sets obtained by the two scan modes.

5.4. *Whole powder pattern and continuity of data sets*

Figs. 5(*a*) and 5(*b*) show the diffraction patterns of Mg_2SiO_4 collected by the MDS after (*a*) 1.5 h and (*b*) the completion of the scan (4 h). Patterns collected with five detectors are represented by five different colours. Fig. 5(*c*) shows the lower part of Fig. 5(*b*) on an enlarged scale. It demonstrates the continuity of the background intensity through the five data sets collected with five different MDS arms and a high signal-to-noise ratio. Fig. 6 shows a comparison of three overlapping reflections from Mg_2SiO_4 scanned with (*a*) the MDS and (*b*) an ordinary-type focusing diffractometer, showing a well resolved pattern for the former. The time required for recording the whole powder pattern of Mg_2SiO_4 over a 2θ range of 130° (5° overlap) at a step interval of 0.004° was just 4 h.

5.5. *Whole-powder-pattern decomposition*

Fig. 7 shows a whole-powder-pattern fitting result obtained with *WPPF* for the intensity data of Mg_2SiO_4 (the same data as shown in Fig. 5). As can be seen from the difference plot between the observed and calculated intensities, an excellent fit was obtained: maximum deviations in the difference plot are all within three times the standard deviations derived from counting statistics. Reliability indices (Young, 1995), which were calculated by including the data points in the background region, were $R_p = 10.3$, $R_{wp} = 14.9$, $R_{\rm expected} = 13.9\%$ and $S = 1.07$ (where S is the goodness of fit). The somewhat high values of these R factors are ascribed to low background intensities and the short counting time of just 1 s at each step. The R_{wp} factor is very close to $R_{\rm expected}$, demonstrating little systematic error in whole-powder-pattern fitting.

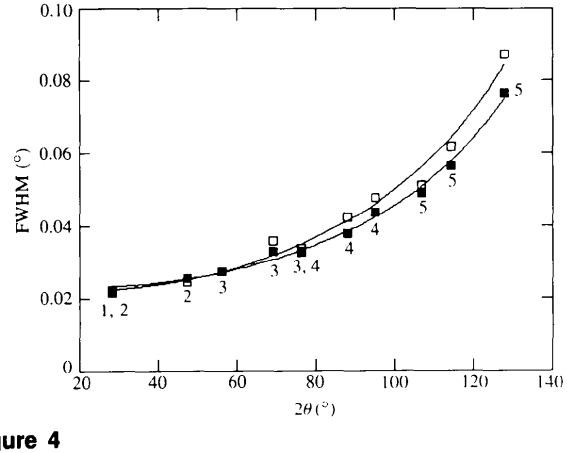

Figure 4
Variations of FWHM of Si with 2θ for data sets obtained using asymmetric 2θ (soiid squares) and symmetric θ–2θ (open squares) scans. Numbers (1 to 5) in the diagram correspond to those of the arms in the multiple-detector system (Fig. 1).

The functional value of the fitted polynomial background decreased from 20 counts at $2\theta = 15°$ to an almost constant value of 15 ± 3 counts through the whole 2θ range, giving a maximum peak-to-background ratio of more than 500. The FWHM was given by $H(2\theta) = (0.00079\tan^2\theta + 0.00052\tan\theta + 0.00039)^{1/2}$, which varied from 0.022° at 17.39° 2θ for the (020) reflection to 0.069° at 127.94° for the (185) reflection. The whole powder pattern could be decomposed with no constraint on intensity parameters such as for equipartition.

5.6. *Rietveld refinement*

Preliminary refinement of only the profile parameters for the Mg_2SiO_4 pattern gave an R_{wp} factor of 19.0%, which was higher than that in the *WPPF* refinement by 4.1%. The difference plot at this stage showed spikes for some strong reflections, which had large positive values for reflections with scattering vectors along the [010] direction and large negative values for directions perpendicular to [010]. These differences between the observed and calculated integrated intensities were considered to arise from the preferred orientation and/or large particles in the specimen. Supplementary observations of the specimen with a scanning electron microscope revealed the presence of large particles (>20 μm) among the small ones (≃1 μm). The intensity variation due to the specimen effect was corrected by including Y_{20} and Y_{22+} terms in the function for symmetrized harmonics expansion (Järvinen, 1993), and R_{wp} was reduced to 16.5%. Inclusion of three additional terms, Y_{40}, Y_{42+} and Y_{44+}, into the refinement reduced R_{wp} a little further to 16.2% ($R_{\rm Bragg} = 6.48\%$). All structural parameters of Mg_2SiO_4 were then refined together with the profile parameters. They converged smoothly, resulting in reliability indices $R_p = 11.8$, $R_{wp} = 15.9$, $S = 1.14$, $R_{\rm Bragg} = 5.98$, $R_F = 4.72\%$. A final fit of the Rietveld refinement is shown in Fig. 8. Refined structural parameters are compared with those for single-crystal data in Table 2.

Refined positional parameters are in good agreement with single-crystal data for Mg^{2+} and Si^{4+} ions. The differences between the present and single-crystal studies are 0.01–0.02 Å for the y coordinates of O^{2-}, and these deviations will be related with relatively large differences between the observed and calculated integrated intensities for the reflections with scattering vectors along [010]. As can be seen from the difference plot for Rietveld refinement

(Fig. 8), both positive and negative deviations still remain in each segment of the whole pattern on the low-angle side, whilst they are absent in the difference plot for *WPPF* refinement. Therefore, a bias on the positional parameters of O^{2-} is considered to arise not from the present detector system but from the specimen.

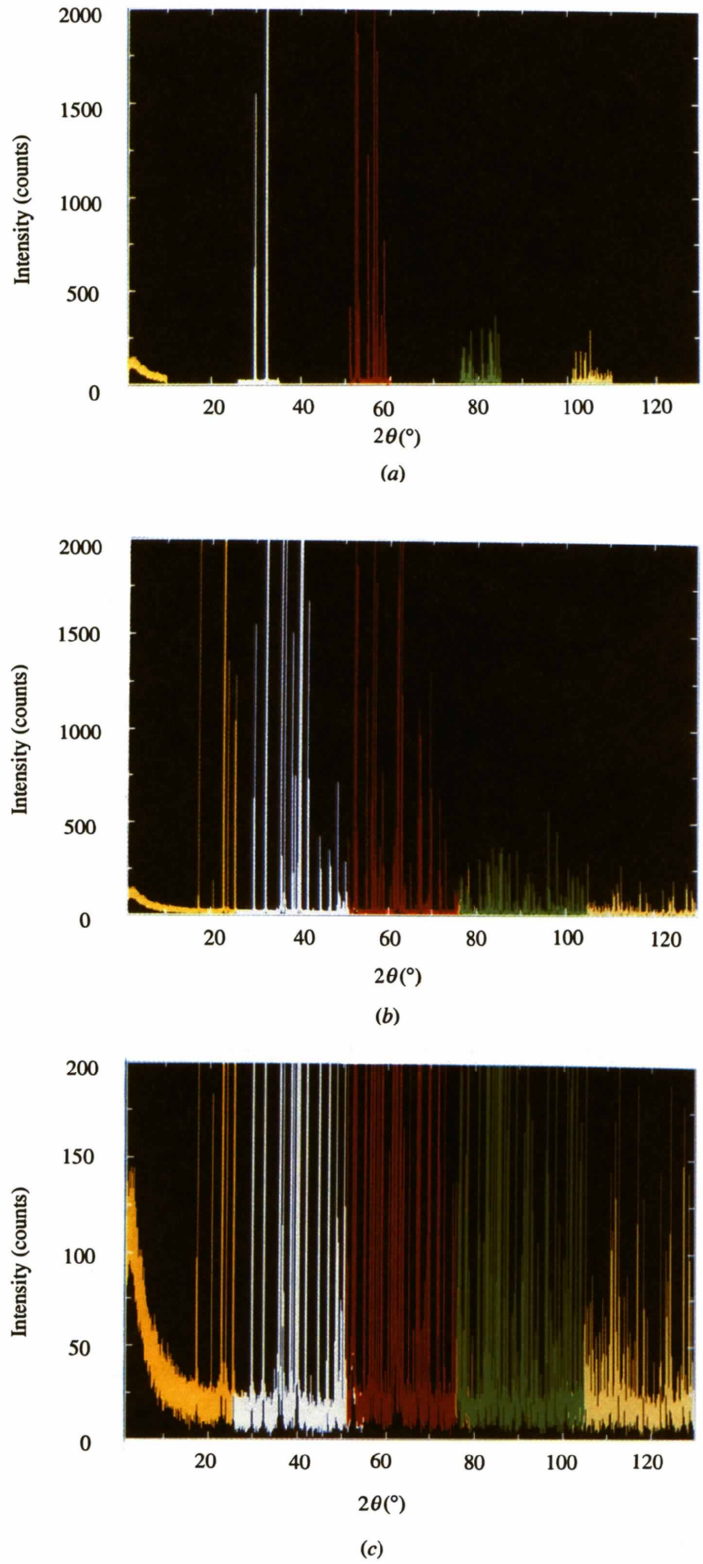

Figure 5
Power diffraction patterns of Mg_2SiO_4 collected using the multiple-detector system after (*a*) 1.5 h, and (*b*) the completion of the scan (4 h). (*c*) The lower part of (*b*) on an enlarged scale. Patterns collected with different detectors are represented by five different colours.

6. Discussion

Multiple-detector systems have been used as standard devices in high-resolution neutron powder diffraction. Their optics are, however, based on Debye–Scherrer geometry, in which absorption of the neutron beam by sample materials is negligible. On the other hand, the present MDS is based on the flat-specimen reflection geometry using a parallel beam, and the high-angular resolution could be achieved by using asymmetric 2θ scanning at a fixed incident angle. In asymmetric diffraction, the height of the diffracted beam increases by $h_{in}\sin(2\theta - \alpha)/\sin\alpha$, where h_{in} is the height of the incident beam, whereas it is identical to h_{in} in symmetric diffraction. Thus, long analyzer crystals are required for asymmetric diffraction. This diffraction mode has, however, several merits: (i) the powder particles in a constant irradiated area and at a constant X-ray penetration depth are involved in the diffraction process during the scan (Toraya *et al.*, 1993*b*), (ii) better particle statistics can be obtained by maximizing the irradiated specimen area at the optimum incident angle, and (iii) the intensity is almost doubled, at the maximum, when compared with that in symmetric diffraction.

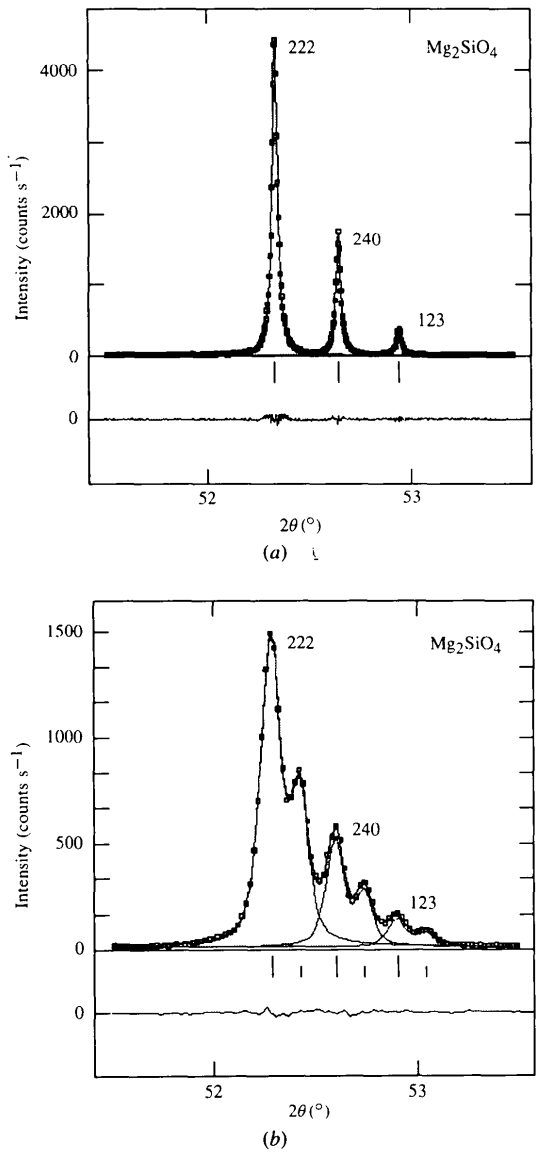

Figure 6
Parts of diffraction patterns of Mg_2SiO_4, collected by (*a*) the present diffractometer, and (*b*) the ordinary-type diffractometer using tube-generated X-rays.

Table 2
Comparison of the structural parameters of Mg_2SiO_4 obtained by Rietveld refinement with those from single-crystal work.

Atom	*x*	*y*	*z*	*B**
Mg(1)	0	0	0	0.36 (2)
	0	0	0	0.38
Mg(2)	0.9913 (2)	0.2776 (1)	1/4	0.33 (2)
	0.9915 (1)	0.2774 (1)	1/4	0.42
	−0.0002	0.0002		
Si	0.4260 (1)	0.0942 (1)	1/4	0.17 (1)
	0.4265 (1)	0.0940 (1)	1/4	0.28
	−0.0005	0.0002		
O(1)	0.7633 (3)	0.0905 (1)	1/4	0.59 (4)
	0.7658 (1)	0.0917 (1)	1/4	0.39
	−0.0025	−0.0012		
O(2)	0.2229 (3)	0.4481 (1)	1/4	0.17 (3)
	0.2218 (1)	0.4471 (1)	1/4	0.39
	0.0011	0.0010		
O(3)	0.2780 (2)	0.1611 (1)	0.0326 (2)	0.29 (2)
	0.2774 (1)	0.1631 (1)	0.0331 (1)	0.46
	0.0006	−0.0020	−0.0005	

Values by obtained by Rietveld refinement are given on the first line and those from single-crystal work (Lager, Ross, Rotella & Jorgensen, 1981) on the second line. The differences between the two values are given on the third line. The unit-cell parameters of Mg_2SiO_4 are a = 4.76595 (5), b = 10.241118 (6), c = 5.99967 (6) Å (Toraya & Ochiai, 1994). * B is the isotropic temperature factor equivalent to a given anisotropic temperature factor (Hamilton, 1959).

In the *ab initio* structure determination using powder data, the powder pattern is first decomposed to obtain integrated intensities of individual reflections. Final structural parameters are, however, ordinarily refined by the Rietveld method using profile intensity data (Rietveld, 1969). In structure refinement using powder data, the Rietveld method is straightforward and powerful, particularly when many peaks are coalescent as in the cases of structures with low symmetry, samples containing extra phases, or samples giving line-broadening effects. However, if the sample gives an almost flat background level and well resolved peaks up to the high-angle region, as shown in Fig 5(*c*), the background level and integrated intensities can be easily and accurately determined using the whole-powder-pattern decomposition method (Pawley, 1981; Toraya, 1986). Then, the so-called two-step method using integrated intensities (Will, 1979) can be used as an alternative means of structure refinement. By changing the observed data from the profile intensities to the integrated intensities, the number of observations used for structure refinement will be reduced to 1/50–1/100, and the structure can be analyzed in the same manner as that of a single-crystal technique.

The MDS can measure the high-resolution diffraction pattern in a moderate scan time, and it is expected to greatly improve the cost–performance of intensity data collection using synchrotron radiation.

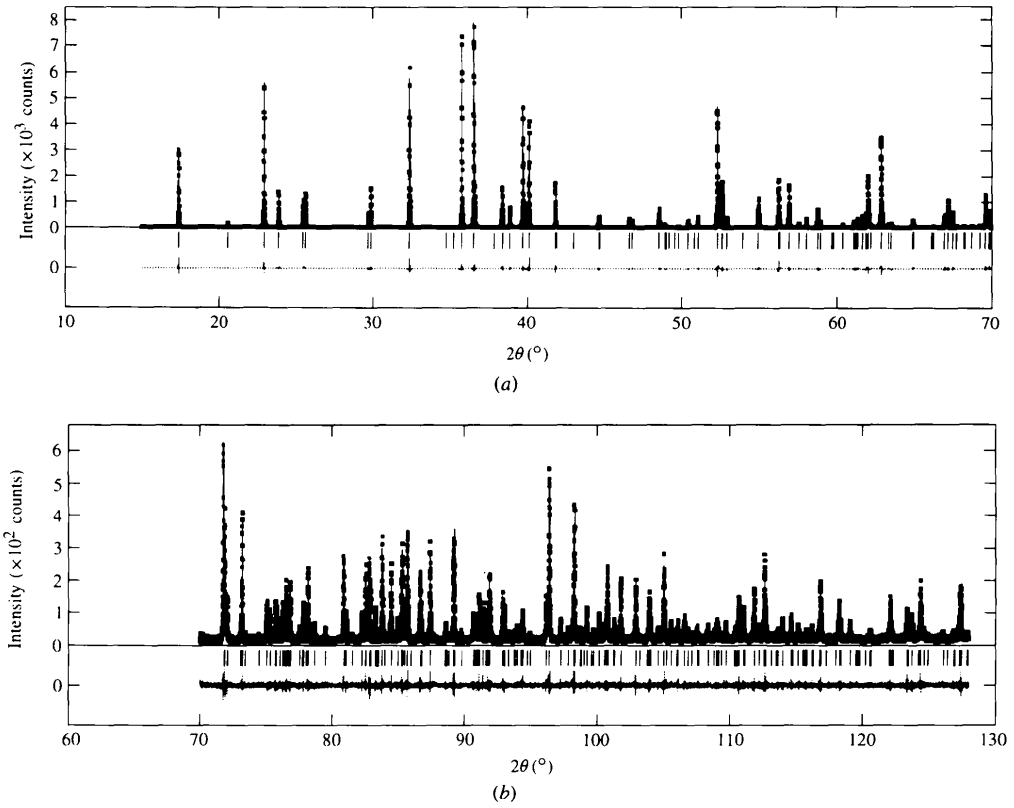

Figure 7
Fit for the *WPPF* refinement of the Mg_2SiO_4 pattern. Half of the diagram (the high-angle side) is represented on an enlarged scale. Solid squares represent observed profile intensity, solid lines the calculated profile intensity and short vertical bars the Bragg reflection positions. The difference between the observed and calculated intensities is given at the bottom of each diagram.

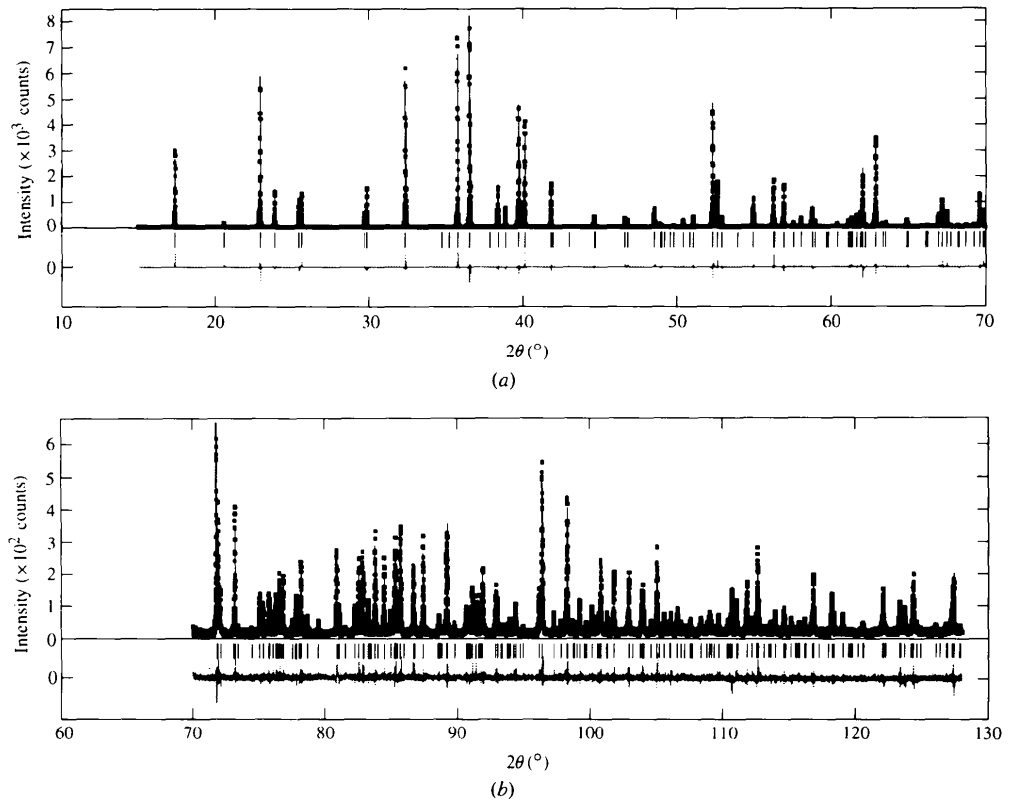

Figure 8
Fit for the for Rietveld refinement of the Mg_2SiO_4 pattern. For details, see Fig. 7.

The present study was financially supported by a Grant-in-Aid for General Scientific Research (No. 06402020) from the Ministry of Education, Science and Culture of Japan. The authors are indebted to the staff of the Photon Factory for their aid and for making the facilities available.

References

Barnea, Z., Creagh, D. C., Davis, T. J., Garrett, R. F., Janky, S., Stevenson, A. W. & Wilkins, S. W. (1992). *Rev. Sci. Instrum.* **63**, 1069–1072.

Caglioti, G., Paoletti, A. & Ricci, F. P. (1958). *Nucl. Instrum.* **3**, 223–228.

Cox, D. E. (1992). *Synchrotron Radiation Crystallography*, pp. 186–254. New York: Academic Press.

Cox, D. E., Hastings, J. B., Cardoso, L. P. & Finger, L. W. (1986). *Mater. Sci. Forum*, **9**, 1–20.

Estermann, M. A. & Gramlich, V. (1993). *J. Appl. Cryst.* **26**, 396–404.

Evain, M., Deniard, P., Jouanneaux, A. & Brec, R. (1993). *J. Appl. Cryst.* **26**, 563–569.

Finger, L. W., Cox, D. E. & Jephcoat, A. P. (1994). *J. Appl. Cryst.* **27**, 892–900.

Hamilton, W. C. (1959). *Acta Cryst.* **12**, 609–610.

Hart, M. (1991). *Mater. Sci. Forum*, **79–82**, 447–454.

Hart, M. (1992). *Adv. X-ray Anal.* **35**A, 329–332.

Hart, M., Cernik, R. J., Parrish, W. & Toraya, H. (1990) *J. Appl. Cryst.* **23**, 286–291.

Hart, M., Parrish, W., Bellotto, M. & Lim, G. S. (1988). *Acta Cryst.* A**44**, 193–197.

Hastings, J. B., Thomlinson, W. & Cox, D. E. (1984). *J. Appl. Cryst.* **17**, 85–95.

International Tables for X-ray Crystallography (1974). Vol. IV. Birmingham: Kynoch Press. (Present distributor Kluwer Academic Publishers, Dordrecht.)

Järvinen, M. (1993). *J. Appl. Cryst.* **26**, 525–531.

Kobayashi, Y. (1992). *Adv. X-ray Anal.* **35**A, 383–391.

Lager, G. A., Ross, F. K., Rotella, F. J. & Jorgensen, J. D. (1981). *J. Appl. Cryst.* **14**, 137–139.

Parrish, W. (1992). *International Tables for Crystallography*, Vol. C, pp. 42–79. Dordrecht: Kluwer Academic Publishers.

Parrish, W. & Hart, M. (1987). *Z. Kristallogr.* **179**, 161–173.

Pawley, G. S. (1981). *J. Appl. Cryst.* **14**, 357–361.

Rietveld, H. M. (1969). *J. Appl. Cryst.* **2**, 65–71.

Tokonami, M. (1965). *Acta Cryst.* **9**, 486.

Toraya, H. (1986). *J. Appl. Cryst.* **19**, 440–447.

Toraya, H. (1990). *J. Appl. Cryst.* **23**, 485–491.

Toraya, H., Huang, T. C. & Wu, Y. (1993*a*). *Adv. X-ray Anal.* **36**, 609–616.

Toraya, H., Huang, T. C. & Wu, Y. (1993*b*). *J. Appl. Cryst.* **26**, 774–777.

Toraya, H. & Marumo, F. (1980). *Rep. Res. Lab. Engin. Mater. Tokyo Inst. Technol.* **5**, 55–64.

Toraya, H. & Ochiai, T. (1994). *Powder Diffr.* **9**, 272–279.

Toraya, H., Takata, M., Hibino, H., Yoshino, J. & Ohsumi, K. (1995). *J. Synchrotron Rad.* **2**, 143–147.

Will, G. (1979). *J. Appl. Cryst.* **12**, 483–485.

Young, R. A. (1995). *The Rietveld Method*, pp. 1–38. Oxford University Press.